Experimental and numerical investigations on the impact behaviour of pristine and patch-repaired composite laminates

H. Liu[1], R.A. Brooks[1], Z.E.C. Hall[1], J. Liu[1], J.W.M Crocker[1], A.M. Joesbury[2], L.T. Harper[2],

B.R.K. Blackman[1], A.J. Kinloch[1,*], J.P Dear[1,*]

[1]*Department of Mechanical Engineering, Imperial College London, South Kensington Campus, London, SW7 2AZ, UK*

[2]*Composites Research Group, University of Nottingham, University Park, Nottingham, NG7 2RD, UK*

*Correspondence to: Professor John P Dear (j.dear@imperial.ac.uk) and Professor Anthony J. Kinloch (a.kinloch@imperial.ac.uk)

Abstract

The present paper investigates the impact behaviour of both pristine carbon-fibre reinforced-plastic (CFRP) composite laminates and repaired CFRP laminates. For the patch-repaired CFRP specimen, the pristine CFRP panel specimen has been damaged by cutting out a central disc of the CFRP material and then repaired using an adhesively-bonded patch of CFRP to cover the hole. Drop-weight, impact tests are performed on these two types of specimens and a numerical elastic-plastic (E-P), three-dimensional (3-D) damage model is developed and employed to simulate the impact behaviour of both types of specimen. This numerical model is meso-scale in nature and assumes that cracks initiate in the CFRP at a nano-scale, in the matrix around fibres, and trigger sub-micrometre intralaminar matrix cracks during the impact event. These localised regions of intralaminar cracking then lead to interlaminar, i.e. delamination, cracking between the neighbouring plies which possess different fibre orientations. These meso-scale, intralaminar and interlaminar, damage processes are modelled using the numerical finite-element analysis (FEA) model with each individual ply treated as a continuum. Good agreement is found between the results from the experimental studies and the predictions from the numerical simulations.

Keywords

Bonded repairs, Composite laminates, Failure analysis, Impact damage, Numerical modelling

1. **Introduction**

Composite materials, especially carbon-fibre reinforced-plastic (CFRP) composite laminates, are widely used in aerostructures, primarily due to their excellent stiffness-to-weight and strength-to-weight ratios. Currently, these materials are being predominantly used in secondary structures, although with the development of the 'Boeing 787' and 'Airbus A350' aircraft they are increasingly being employed in primary structures. However, an area of particular concern when considering the performance of composite laminates, such as CFRPs, for aircraft structures is the impact performance of the composite laminate. Especially since the damage induced in the composite by the impact event may not be readily visible but may grow in extent, if left unrepaired, upon further loading under impact and/or cyclic-fatigue stresses and may eventually cause failure of the composite laminate.

Now, such impact events may arise, for example, from dropped tools, bird strikes, hail stones, runway debris, airport equipment striking the fuselage and hard landings and any such induced damage in the CFRP laminate needs to be repaired to prevent its further growth [1-3]. Therefore, the main aims of the present work are to investigate the impact behaviour of (a) pristine carbon-fibre reinforced-plastic (CFRP) composite laminates and (b) repaired CFRP laminates where the pristine laminates have been damaged and then repaired using an adhesively-bonded patch of CFRP. In the present paper, drop-weight, impact tests are performed on the pristine CFRP panels and patch-repaired CFRP laminates and an elastic-plastic (E-P), three-dimensional (3-D) damage numerical model is developed and employed to simulate the impact behaviour of both the pristine and the repaired laminates.

The damage that typically develops in a composite laminate upon being impacted originates from nano-scale defects and Clyne and Hull [4] have demonstrated very clearly how the fibre/matrix interface in a composite, and the polymeric matrix immediately surrounding the individual fibres, can lead to nano-scale cracks being present. Furthermore, from a study by Neogi et al. [5], it appears that the triaxial stress-state near a fibre-matrix interface plays a significant role in such cracking processes, leading to cavitation on a nano-scale. Features on the fibre, due to its surface roughness, with a length-scale of the order of 50-100 nm, and the presence of sizing on the fibre surface can also play a role in the initiation processes of nano-scale cracks [6]. Indeed, Kimura et al. [7] have recently developed techniques with a nano-scale spatial resolution for observing such nano-scale crack initiation in composites. Their technique combines phase-contrast X-ray computed tomography and transmission X-ray microscopy, using synchrotron radiation, and they have shown that nano-scale cracks are initiated with a length of approximately 50 nm. Such nano-scale cracks then trigger the development of further damage processes (a) in the polymer matrix as intralaminar matrix cracks and (b) along the fibre/matrix

interfaces as interlaminar cracks. Considering increasing length-scales, Topac et al. [8] and Shi et al. [9] have demonstrated that intralaminar matrix cracks, within a composite ply, develop from these nano-scale defects, and that these meso-scale intralaminar cracks can then be diverted into forming significant interlaminar, i.e. delamination, cracks between the ply interfaces, especially where the fibres have different orientations. Similarly, Davies and Zhang [10] and De Moura and Marques [11] have made the important observation that transverse matrix tensile cracks often may lead to delamination cracking. Finally, Berton et al. [12], Johnson [13] and Sun and Hallett [14] have reported that the critical damage from an impact event on a CFRP laminate, that leads to a loss of mechanical performance and eventual failure of the composite, is primarily this delamination cracking, accompanied by some fibre fracture if very extreme impact-loading occurs.

Based upon the above observations, the novel numerical, finite-element analysis (FEA) model developed in the present paper considers the two distinct types of meso-scale damage that are typically observed upon impacting a CFRP laminate, namely intralaminar and interlaminar damage. Since it is the development of such meso-scale intralaminar damage, and especially subsequent meso-scale interlaminar damage, that leads to the decrease in the mechanical performance and eventual failure of the damaged composite laminate, as discussed above. In our model, intralaminar damage may consist of plastic deformation of the matrix, matrix cracking, fibre debonding and localised fibre failure. Such intralaminar damage then leads to the initiation and growth of the more important, in the context of the failure of the CFRP laminate, interlaminar damage, i.e. delamination cracking. This latter type of damage typically involves the initiation and growth of interlaminar cracks between the plies that make up the composite laminate and the initiation and growth of such delaminations is particularly likely to occur between the ply interfaces where the fibres have different orientations.

2. Experimental

2.1 Introduction

The experimental details have been described in a recent paper [15] and therefore only a brief overview is given below. In the present work, a single-sided patch-repair technique is used to repair the damaged CFRP laminate. In the patch-repaired specimen the CFRP patch is adhesively-bonded onto the parent CFRP from which the damaged area has been removed. This is a commonly employed technique [2,3,16] and was chosen as it would enable C-scan tests to be performed on the patch and parent material from the front face of the patch and from the rear face of the parent material. A main interest of the present research was to observe delamination development from the drop-weight impact tests,

through the thickness of the patch and through the thickness of the parent material if it occurred. These experimental data may then be employed to verify the results from the modelling, which is a major aim of the present paper. Another benefit of a patch repair is that it can be undertaken on composite components when only one side of the damaged CFRP laminate can be easily accessed.

2.2 Materials and specimens

The panels used for the present research were manufactured using quasi-isotropic CFRPs made from unidirectional prepreg, MTC510-UD300-HS-33%RW supplied by SHD Composite Materials Ltd, UK, with the prepreg having a volume fraction of continuous carbon-fibres of 60%. Flat panels were cured at 110^{o}C for 120 minutes using an autoclave and the glass transition temperature of the cured CFRP was 133°C. The quasi-isotropic lay-up used for the pristine CFRPs panel specimens was $[45_2/-45_2/0_2/90_2]_s$, where the 0° plies were aligned with the longer edge of the panels and the panel had a nominal thickness of 4.58 mm, see Figure 1a. The patch-repaired CFRP specimen, see Figure 1b, was manufactured by removing a 40 mm diameter disk to represent the impact-damaged area, see below, from the centre of a pristine CFRP laminate panel, which now became the 'damaged', parent, CFRP panel. A circular quasi-isotropic CFRP patch, with a lay-up of $[45/-45/0/90]_s$, a diameter, D, of 65 mm and a nominal thickness of 2.29 mm, was then bonded to the parent CFRP to cover the hole. (It should be noted that often the patch is taken to be 1.5 to 2 times the diameter of the cut-out hole to give a relatively large overlap. However, the central unsupported region of the specimen did not allow for this as a standard drop-weight fixture had to be employed and a main aim of the present work was to provide a repair geometry suitable for the drop-weight experiments, so that the impact test results could be compared with the equivalent modelling output.) The adhesive used was a single layer of a toughened epoxy-film adhesive, MTFA-500 from SHD Composite Materials Ltd, UK, which had a nominal thickness of 0.25 mm. The surfaces of the parent and the patch were prepared prior to bonding using 50 grit sanding-discs and were then cleaned with acetone. The adhesive layer was cured at 130°C for 90 minutes.

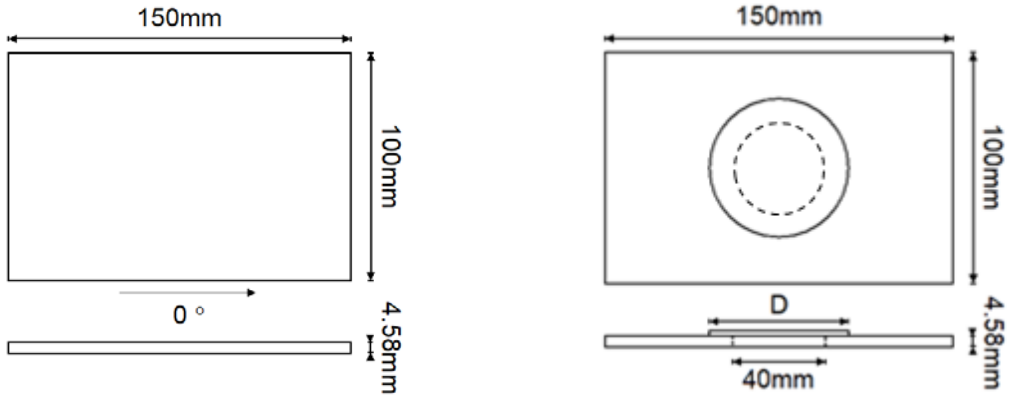

(a) (b)

Figure 1. The plan- and side-views of (a) the pristine CFRP panel specimen and (b) the patch-repaired CFRP specimen where the patch diameter, D, is 65 mm and the removed disc of CFRP from the parent CFRP, shown by the dashed line, is 40 mm in diameter.

2.3 Impact tests

The drop-weight impact experiments were performed using an Instron CEAST 9340 (Italy) tower equipped with an instrumented stainless-steel impactor having a hemispherical head with a diameter of 16 mm, as shown in Figure 2, and has been described in detail previously [15,17]. Both the pristine and patch-repaired specimens were impacted in the centre using an energy level of 7.5 J. The overall mass of the impactor was 5.27 kg and the corresponding impact velocity was 1.69 $m.s^{-1}$. A catching system was used to prevent further impact events from occurring after the initial impact. No software filtering of the signal of the measured load versus time trace was employed and the software for the instrumented drop-weight test provided the impact load and displacement as a function of the time-scale of the impact event. The impacted specimens were inspected [15,17] using a Prisma portable ultrasonic C-scanner, supplied by Sonatest Ltd, UK, to detect any area of interlaminar cracking in (a) the pristine CFRP specimens and (b) the patch-repaired CFRP specimens, and any adhesive cracking present in the latter specimens. (Note that a flat patch with no tapering, also termed scarfing, of the ends of the repair CFRP was employed in the present study. Since C-scan tests can only be performed on flat surfaces and tapering of the ends of the bonded patch would obscure any delaminations in the tapered region.)

Figure 2. The equipment used for the drop-weight impact tests.

3. Numerical modelling

3.1 Overview

For the impact of laminated structures, the initial impact causes a local indentation in the top surface directly under the impactor associated with intralaminar damage, e.g. localised plasticity and matrix cracking, and this is followed by initiation of interlaminar damage e.g. delamination. Where the modulus of each ply layer changes across a ply interface, due to a change in fibre orientation, then the impact load tends to initiate delamination growth at the interface between plies. The delamination tends to grow in the direction of the fibres in the ply beneath the interface, driven by regions of high strain gradient. Thus, upon impacting CFRP laminates two distinct types of meso-scale damage are typically observed: intralaminar and interlaminar damage. Intralaminar damage may consist of plastic deformation of the matrix, matrix cracking, fibre debonding and localised fibre failure (at high impact energies). Such intralaminar damage often leads to the initiation and growth of the more important interlaminar damage e.g. delamination. This is especially important as it can lead to subsequent fatigue failure of the CFRP laminate, as noted above. This latter type of damage typically involves the initiation and growth of delaminations, i.e. interlaminar cracking, between the plies that make up the composite laminate. The implementation of the elastic-plastic (E-P), three-dimensional (3-D) finite-element analysis (FEA) model

that was employed to predict the meso-scale intralaminar and interlaminar damage suffered by the CFRP composite in the pristine and the patch-repaired specimens, and any adhesive cracking in the latter specimens, during the impact event is shown schematically in the flowcharts in Figure 3. The FEA model was created for both the pristine CFRP and the repaired CFRP composite specimens in 'ABAQUS 2018' (supplied by Dassault Systemes, Providence, Rhode Island, USA). This overall flowchart in Figure 3 is for one computational time-step and a single integration point. All the methodologies and equations that are used in the numerical FEA model, as given in this figure, are derived and presented in [18], where they are numbered as in Figure 3. Indeed, it should be noted that [18] gives the full details of the model, extended in the present paper to the repaired CFRP panels, that has been proposed and previously verified for the impact of pristine composite panels. In this paper [18], all the equations may be found that are given in Figure 3, using the same numbering system, along with all the terms defined and used in the equations. Also, in [18] the reader can follow the logical development of the model, the failure criteria used and how crack initiation and propagation for the intralaminar and interlaminar damage regions are defined and quantitatively modelled.

3.2 The finite element analysis (FEA) model

The meshes used for the FEA modelling of (a) the pristine CFRP specimen and (b) the patch-repaired CFRP specimen studies are illustrated in Figure 4. In the pristine specimen, the composite plies were modelled using 1.5 mm × 1.5 mm C3D8R elements. In the patch-repaired specimen, the CFRP parent panel was modelled using 3 mm × 3 mm C3D8R elements and the CFRP patch was modelled using 1.5 mm × 1.5 mm C3D8R elements. The total number of elements employed was 56,434 and 67,640 for the pristine and the patch-repaired specimens, respectively. The adhesive layer in the patch-repaired specimen was modelled using 1.5 mm × 1.5 mm C3D8R elements and the number of elements was 8,432. The exuded 'spew fillet' of the adhesive layer was modelled as shown in Figure 4b. Two elements were employed in the through-thickness direction of each composite ply and the adhesive layer, and the elements were shaped as needed to better fit the rounded contours present in the patch-repaired specimens. These meshes delivered mesh-independent results with good accuracy whilst ensuring a good overall computational efficiency. The general contact algorithm was employed for the global contact and the cohesive surface solution was used for both the composite/composite interface and the composite/adhesive interface [18]. The boundary condition of the FEA model was defined according to the test set-up as employed in the impact experiments. Friction coefficients of 0.2 and 0.25 were defined in the global contact and cohesive contact, respectively [18]. Computation accuracy was set as 'double procession' to reduce the accumulation of errors during running the simulation. The flow-chart for the

implementation of the finite element model is schematically shown in Figure 3, giving a typical computation step for a single element with the various options for the damage processes being run simultaneously. The computation process was performed for every appropriate single element in the model. Computations were undertaken using 16 CPUs on a Linux Cluster with a run time of 27 to 35 hours. In the FEA model the basic mechanical properties, as defined in [18], of the composite ply and the adhesive layer, including strengths, moduli and fracture toughness, etc., that were required were obtained from the manufacturer's data sheets and from the literature [18,19-24], and the non-linear parameters reported in [18] were taken for the CFRP. The input parameters employed for the FEA model, taken from the literature [18,19-24], are given in Table 1.

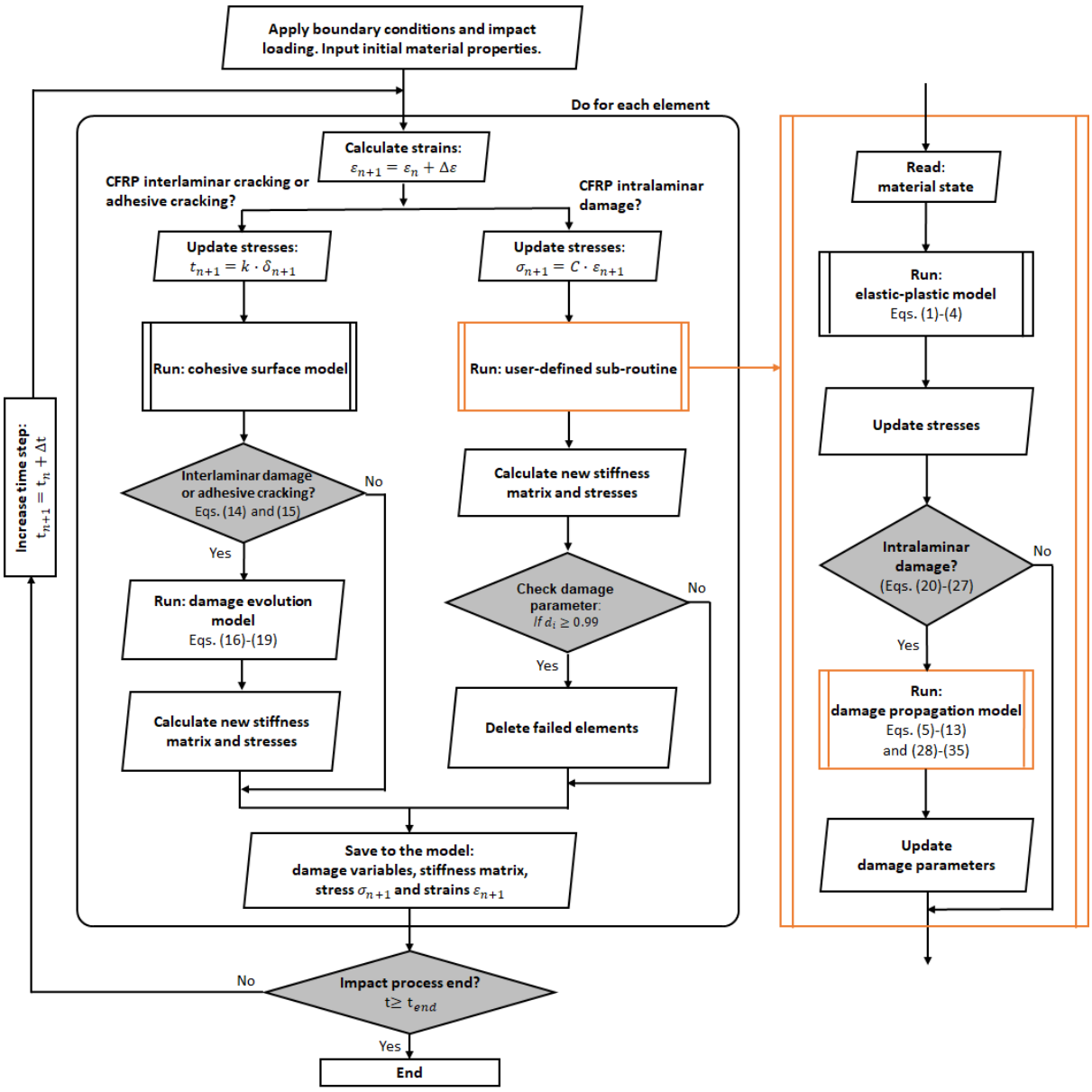

Figure 3. The implementation of the E-P, 3-D FEA numerical damage model showing schematically the overall flowchart for one computational time-step and a single integration point. Both the flowcharts for the main model and for the elastic-plastic (E-P) user-defined sub-routine are shown. This FEA modelling simulation of the impact event would be run typically over a time-scale, t, of 0 to ca. 6 ms, with ca. 100 time-steps being employed. The simulation runs were stopped when the defined total computation time for the impact simulation event had expired. (All the methodologies and equations that are used in the above FEA model are derived and presented in [18], where they are numbered as above.)

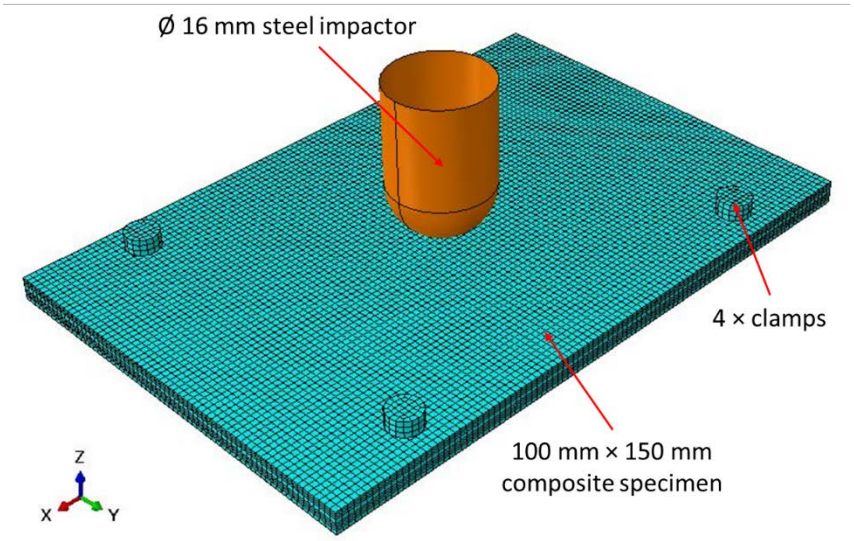

(a)

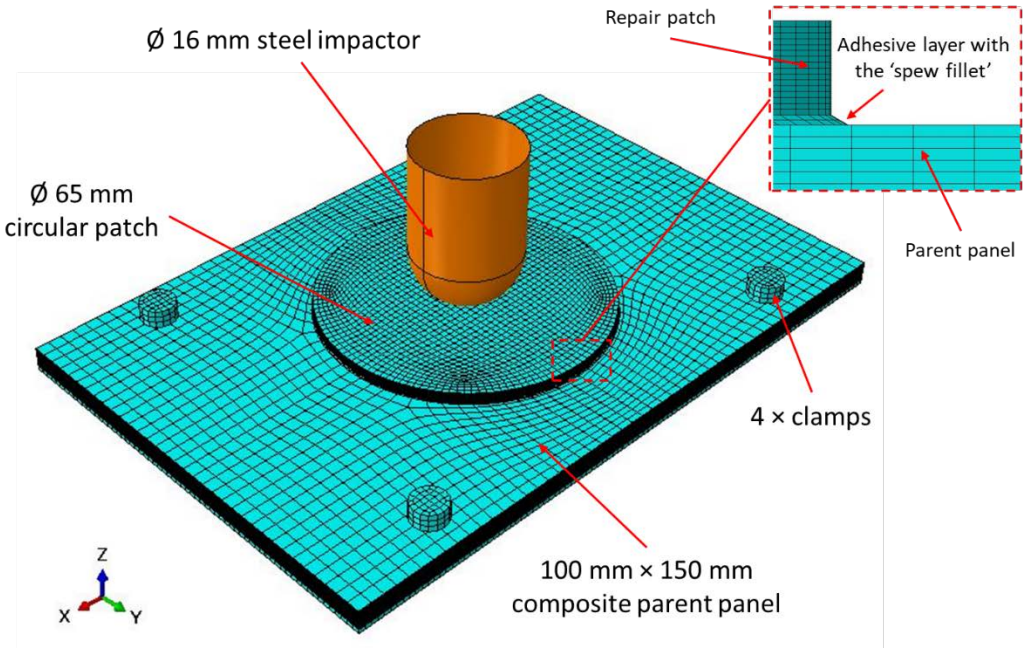

(b)

Figure 4. The finite-element analysis (FEA) model for simulating the impact event on: (a) the pristine CFRP specimen and (b) the patch-repaired CFRP specimen.

Table 1. The properties, as defined in [18], of the unidirectional CFRP and the rubber-toughened adhesive used in the FEA modelling studies [18,19-24].

Property	CFRP	Adhesive
Moduli (GPa)	$E_{11} = 115;\ E_{22} = E_{33} = 8.2$ $G_{23} = 3.6;\ G_{12} = G_{13} = 3.6$	$E = 2.1$
Poisson`s ratio	$\nu_{23} = 0.34;\ \nu_{12} = \nu_{13} = 0.34$	$\nu = 0.3$
Strength, *S*, values (MPa)	$S_{1t} = 2282;\ S_{2t} = S_{3t} = 54$ $S_{1c} = 1067;\ S_{2c} = S_{3c} = 200$ $S_{12} = S_{13} = S_{23} = 99$	
Intralaminar ply fracture energies ($\mathrm{kJ/m^2}$)	$G_{Ic}\vert_{ft} = 133;\ G_{Ic}\vert_{fc} = 40$ $G_{Ic}\vert_{mt} = 0.4;\ G_{Ic}\vert_{mc} = 1.3;\ G_{IIc}\vert_{ms} = 1.3$	
Interlaminar ply or adhesive fracture energies ($\mathrm{kJ/m^2}$)	$G_{Ic} = 0.4;\ G_{IIc} = 1.3$	$G_{Ic} = 2.3;\ G_{IIc} = 2.8$
Benzeggagh–Kenane exponent	$\eta = 1.45$	$\eta = 1.45$
Cohesive strengths (MPa)	$t_{33}^0 = 43.0;\ t_{31}^0 = t_{32}^0 = 50.0$	$t_{33}^0 = t_{31}^0 = t_{32}^0 = 45.0$
Initial cohesive law stiffness (MPa/mm)	$k_i = 6.4 \times 10^5$	$k_i = 6.4 \times 10^5$
E-P model: coefficient, a_{66}, and material constants, A and n	$a_{66} = 2.7;\ A = 3.14\ x\ 10^{-13}\ \mathrm{MPa}^{-n}$; $n = 4.19$	

4. Results and discussion

4.1 Introduction

The experimental and numerical modelling results for (a) the load versus time and (b) the load versus displacement curves are first discussed, followed by the results relating to the energy loss of the impactor versus time curves. Finally, the type, shape and location of the impact-induced damage that has resulted in both the pristine CFRP specimen and the patch-repaired CFRP specimens are considered, and the experimental results are again compared with the predictions from the simulations using the numerical FEA model, described in Section 3.

4.2 Load versus time and load versus displacement curves

Figures 5 and 6 show a comparison between the load versus time curves and the load versus (out-of-plane) displacement curves, respectively, obtained from the impact experiments and the E-P, 3-D FEA simulations for (a) the pristine CFRP specimens and (b) the patch-repaired CFRP specimens, respectively. Several interesting points arise. Firstly, duplicate experimental tests were conducted for each type of specimen and the agreement between the replicate tests is very good. Secondly, for both types of specimen, the overall load response, i.e. the maximum loads, impact duration times and maximum out-of-plane displacements, are effectively captured by the predictions from the FEA simulations. Thirdly, the relatively small amplitude, sinusoidal oscillations on the initially-rising part of the load versus time experimental curves are indicative of mass-spring oscillations, as first analysed in detail in [25-29]. Fourthly, in Figure 5 the initiation load for interlaminar damage to occur, i.e. where there is a significant decrease in the load, is higher and more distinct for the pristine specimens compared with the repaired specimens. This significant load drop is indicative of the initiation of damage in the composite and is often accompanied by oscillations after the load drop. This initiation of damage, as marked by a significant load decrease and subsequent oscillation, is often associated with the initial failure, e.g. plastic indentation, intralaminar and subsequent delamination, of the CFRP that occurs under an impact load and has been described in detail by Liu et al. [18] and Bienias et al. [29]. The measured initiation load for the pristine specimens is approximately 4.5 kN, whilst that for the repaired specimens is approximately 1.7 kN. The modelling results also give a higher load for the initiation of damage in the pristine specimen: occurring at approximately 2.7 kN for the pristine specimen compared with approximately 2.0 kN for the repaired specimen. The difference between these values for the initiation load for the pristine and patch-repaired specimens, as observed from both the experiments and the modelling simulations, arises because the CFRP repair patch is relatively thin compared to the CFRP pristine specimen and is therefore more compliant. Thus, the patch-repaired specimen has a lower contact stiffness and, hence, the damage is introduced at a lower impact load in the case of the patch-repaired specimens. For both the pristine and repaired specimens, this initiation of damage is associated with a significant decrease in the gradient of the load versus displacement curves, see Figure 6, as has been previously observed [17,18]. As would be expected from the above comments, this decrease in the gradient of the load versus displacement curves is more marked for the patch-repaired specimens compared with the pristine specimens. Finally, however, it is apparent that the onset of damage from the simulation of the pristine samples occurs at a somewhat lower load than in the experiments, see Figures 5a and 6a. However, the maximum load, maximum displacement and the

duration of the impact event are quite well predicted by the simulation when compared with the experimental results. Also, the extent of delamination damage for the simulation is in good agreement with the experimental C-scan images (see Figure 8 later). The decrease in the load associated with the onset of damage shows similar features in the modelling as in the experiments, e.g. a sharp load drop followed by oscillations. This initial load-drop associated with the onset of damage is influenced by many factors, as it is linked to the initial indentation beneath the impactor, where localised plasticity and matrix cracking occurs. For this reason, it is not unusual for the load for the onset of damage to be slightly different in value as determined from the simulations and the experiments.

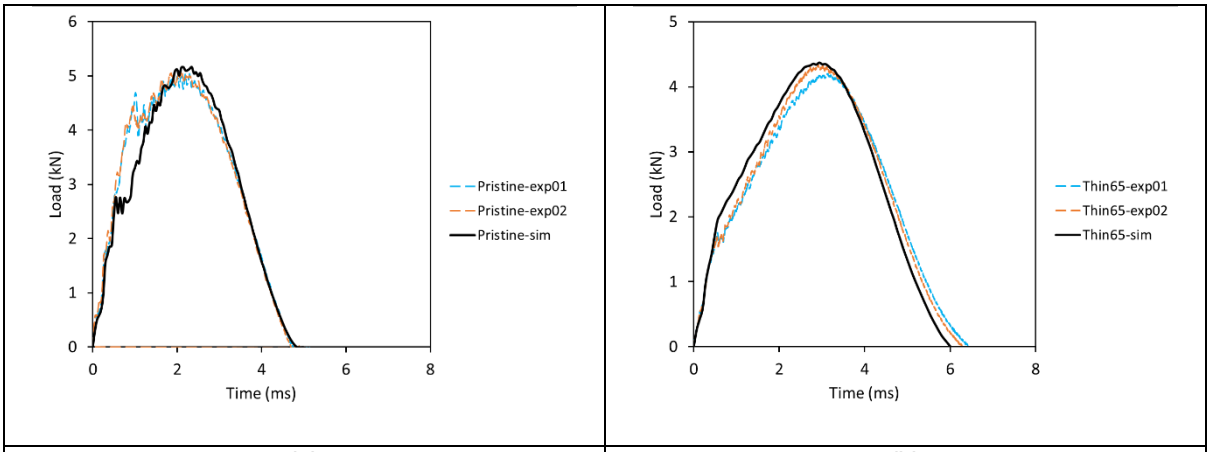

(a) (b)

Figure 5. The experimental and predicted load versus time curves obtained from:
(a) the pristine CFRP specimens and (b) the patch-repaired CFRP specimens.

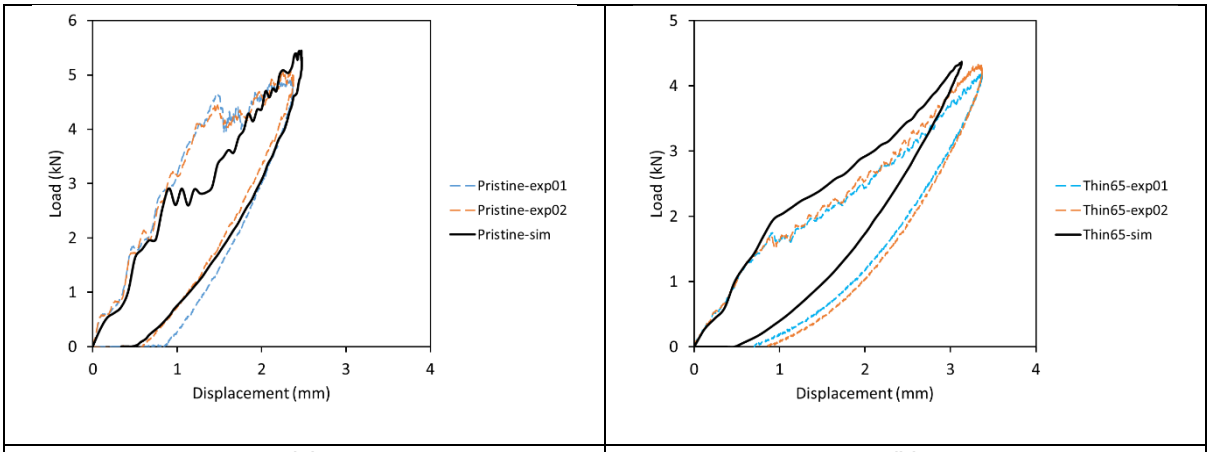

(a) (b)

Figure 6. The experimental and predicted load versus displacement curves obtained from:
(a) the pristine CFRP specimens and (b) the patch-repaired CFRP specimens.

4.3 Energy loss of the impactor versus time curves

Figure 7 demonstrates that there is an appreciable energy loss of the impactor upon striking both the pristine and repaired specimens, which is of the order of 50%. This energy loss, which is also accurately modelled using the E-P, 3-D FEA simulations, is mainly associated with the initiation and propagation of damage processes in the pristine CFRP specimens and the CFRP patch of the repaired CFRP specimens, i.e. plastic deformation of the composite material and intralaminar and interlaminar cracking in the CFRP, as discussed below. The plastic deformation mainly occurs relatively locally around the impact site, where an indentation under the round-nosed impactor arises from the plastic deformation of the matrix. Further intralaminar damage, e.g. matrix cracking, also occurs under the impactor, which subsequently develops into the more significant damage process of interlaminar cracking.

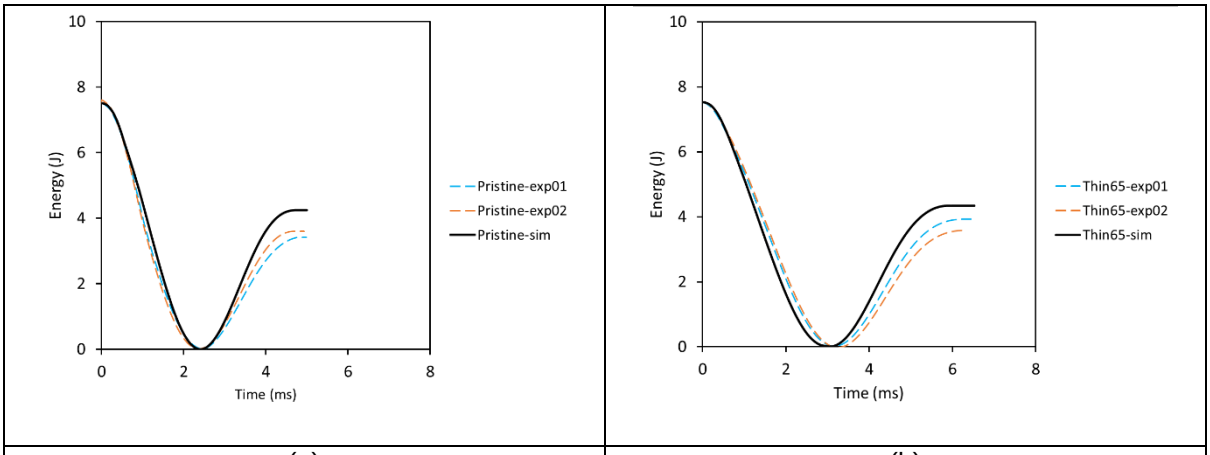

(a) (b)

Figure 7. The experimental and predicted impactor kinematic energy versus time curves obtained from impact tests on: (a) the pristine CFRP specimens and (b) the patch-repaired CFRP specimens.

4.4 Impact damage

4.4.1 Introduction

The impacted specimens were inspected using ultrasonic C-scanning to detect any area of interlaminar cracking, i.e. delaminations, in the CFRP laminate in (a) the pristine specimens and (b) the patch-repaired specimens, and also any adhesive cracking in the latter specimens. Interlaminar cracking, i.e. delaminations, in the CFRP laminates was detected in both types of specimen, as discussed below. However, there were no indications at all of any adhesive cracking in the patch-repaired specimens and these experimental observations are in agreement with the results from the FEA studies, which indeed predicted that no adhesive cracking would occur in the impacted patch-repaired specimens.

4.4.2 Intralaminar damage in the CFRP laminates

Figures 8a and 9a present the predictions for intralaminar damage in the pristine CFRP and patch-repaired CFRP specimens, respectively, and these figures show cross-sectional views of the predicted intralaminar matrix damage induced by the impact event. The predicted intralaminar damage is shown as 'red-coloured' in these schematic cross-sectional views. As described above, the numerical model is meso-scale in nature, in which cracks initiate in the CFRP at a nano-scale but then develop into meso-scale damage. Such nano-scale cracks and defects [5-7] have been shown to initiate in the matrix around fibres, etc. and these then trigger sub-micrometre intralaminar matrix cracks that initiate and propagate around the impact point. These processes are initially controlled by the plasticity of the matrix and are localised under an indentation that results in the CFRP from the strike by the impactor. Indeed, the intralaminar damage is confined to a region just below the impact site for both the pristine CFRP and the patch-repaired CFRP specimens. It is noteworthy, that for the patch-repaired specimen, see Figure 9a, that the intralaminar damage is predicted to be confined to the CFRP repair patch and no such damage is predicted to occur in the underlying parent CFRP laminate to which the patch is adhesively-bonded.

4.4.3 Interlaminar damage in the CFRP laminates

The localised regions of intralaminar damage discussed above lead onto the initiation and propagation of critical interlaminar damage, i.e. delaminations, which is cracking between the neighbouring CFRP plies which possess different fibre orientations, and such cracking tends to propagate along the orientation of the ply beneath the delamination. Comparisons between the experimental and the predicted footprint areas of the interlaminar cracking obtained for the pristine and patch-repaired CFRP specimens are shown in Figures 8b and 9b. The right-hand side scales in these figures indicate the location of the delaminations as a function of the depth through the thickness of the specimen, where the dark-red colour represents the front (impacted) face and the dark-blue colour represents the rear (non-impacted) face of the composite specimen. The 0^{o} fibre direction is also indicated. The areal footprint of the damage, i.e. the damage area (labelled 'DA'), is given at the bottom left in each case, see Figures 8b and 9b, and this was determined by counting the number of pixels which had a colour that was not dark blue, since the rear surface simply reflects the ultrasound and appears as being dark blue in colour. The predicted interlaminar delaminations from the E-P, 3-D FEA modelling are also colour-coded to give depth information, in the same way as for the experimental data, and a similar

calculation was undertaken for the damage area (DA), as shown in the bottom left of the image. The dashed white line, on both the pristine and patch-repaired samples, represents the 40 mm diameter of the circular hole in the patch-repaired specimens. (The dashed white line is included on the pristine specimen simply to allow a ready comparison with the damage area for both the pristine and patch-repaired CFRP specimens.)

There are several interesting observations from these results on the extent of interlaminar cracking. Firstly, for both the pristine and patch-repaired CFRP specimens, the predicted damage areas for interlaminar cracking from the numerical modelling studies are very similar in value to the experimentally measured values. Indeed, the agreement obtained between the areal values, locations and shapes of the delaminations from the experiments and the FEA simulations clearly again validates the numerical modelling studies. Secondly, the interlaminar damage area (DA) is significantly greater for the patch-repaired CFRP specimens compared with that for the pristine specimens. This is to be expected as the repair CFRP patch (a) is not supported by any plug of material, which would have filled the hole left by removal of the disc of CFRP, and (b) is relatively thin compared to the pristine CFRP panel. Hence, the CFRP patch can deform more easily and so incurs a greater area of interlaminar cracking compared to the pristine CFRP specimen. Thirdly, for the patch-repaired specimens the delamination damage only occurred in the CFRP patch and was limited in extent to the edge of the circular hole beneath the patch. Thus, there was no measured, nor predicted, damage in the parent CFRP, which was situated below the patch and to which it was adhesively-bonded. As stated previously, the main aim of this initial study was to investigate whether a novel numerical model that has been developed could realistically predict the impact behaviour of a CFRP panel that had been repaired with an adhesively-bonded patch. This work has also demonstrated that the bonded CFRP repair patch has fulfilled one of its primary purposes in preventing the initiation and development of interlaminar cracking in the parent CFRP, as was also observed to be the case for intralaminar damage, as discussed above. Notwithstanding, the patch has also to restore the strength of the parent material once the damaged CFRP has been removed and the patch applied. This aspect will be assessed, both experimentally and theoretically, in future work.

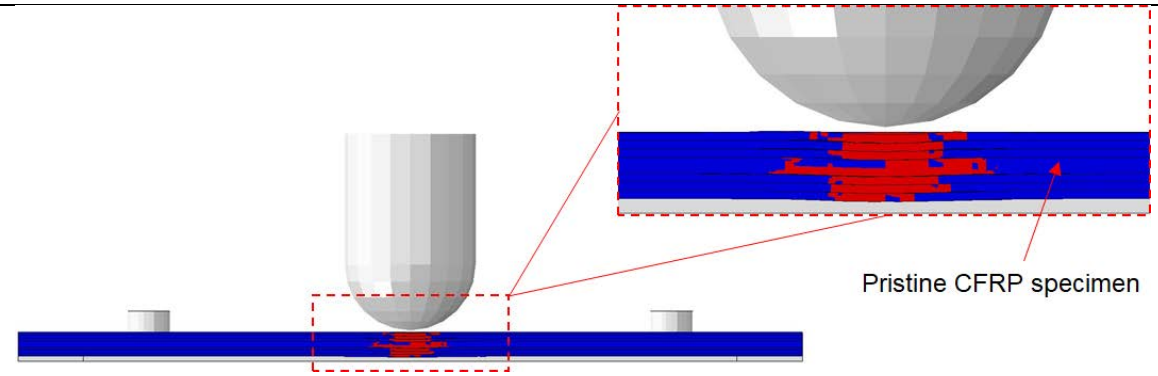

(a)

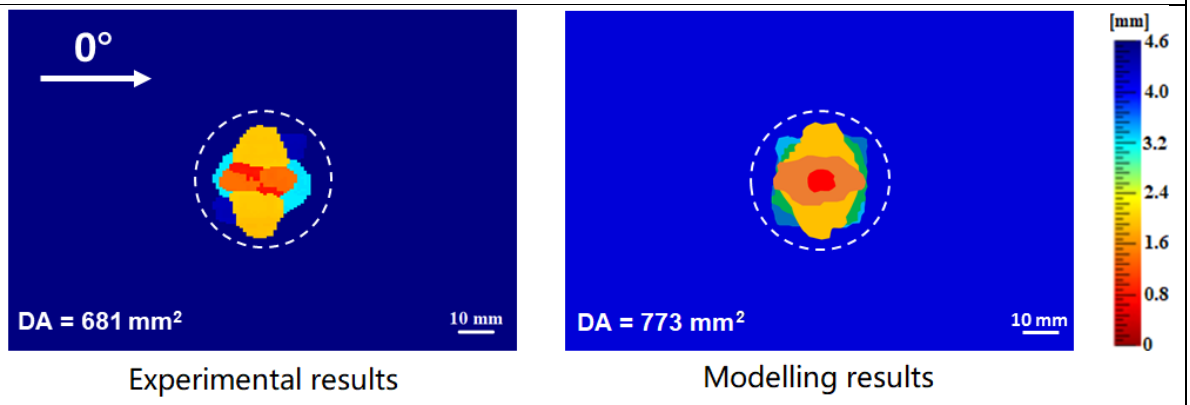

(b)

Figure 8. The impact damage in the pristine CFRP specimens: (a) the intralaminar matrix damage and (b) the interlaminar damage, i.e. delamination cracking. ('DA' is the damage area of the interlaminar cracking footprint. The white dashed lines indicate the area from which the 40 mm disc of CFRP was subsequently cut out.)

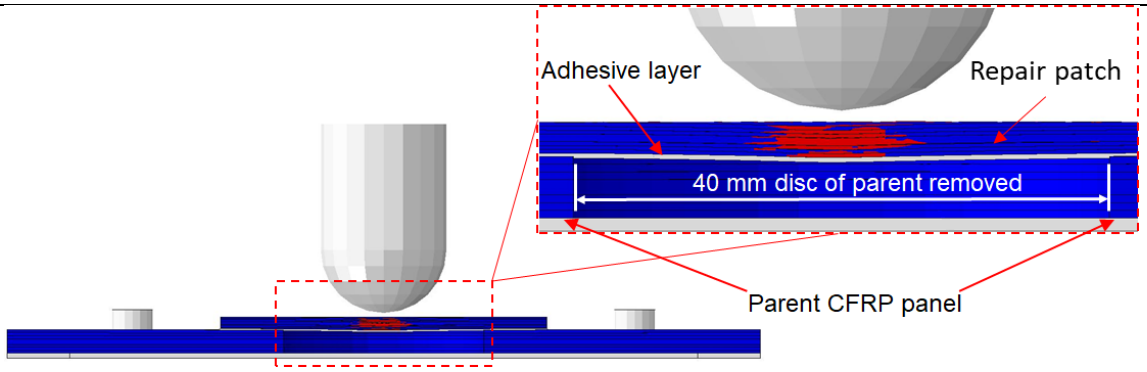

(a)

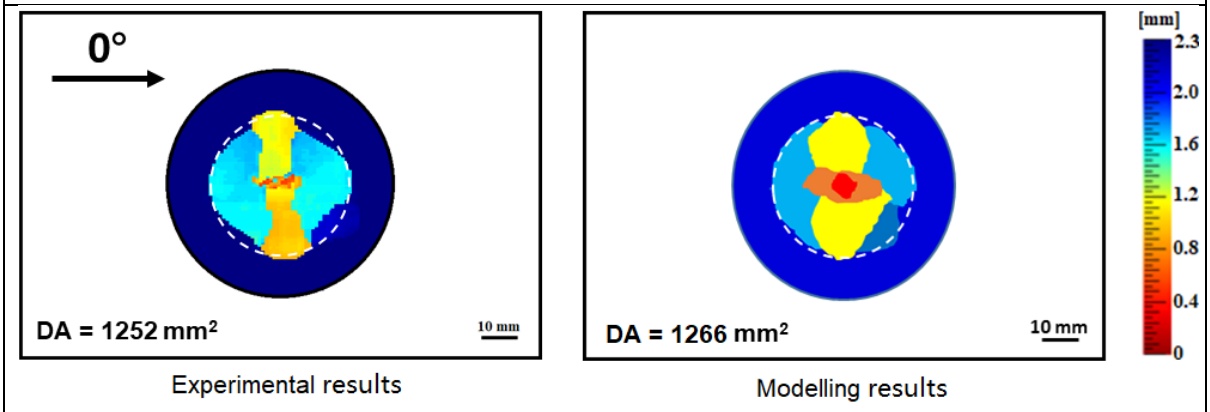

(b)

Figure 9. The impact damage in the patch of the patch-repaired CFRP specimens: (a) the intralaminar matrix damage and (b) the interlaminar damage, i.e. delamination cracking. ('DA' is the damage area of the interlaminar cracking footprint The white dashed lines indicate the area from which the 40 mm disc of CFRP was cut out before the CFRP repair-patch was adhesively-bonded to the parent CFRP.)

5. Conclusions

A three-dimensional (3-D) finite-element analysis (FEA) model incorporating an elastic-plastic (E-P) damage model has been developed to predict accurately the impact behaviour of (a) pristine carbon-fibre fibre-reinforced (CFRP) specimens and (b) patch-repaired CFRP specimens which consisted of an adhesively-bonded patch of CFRP bonded over a hole present in the parent CFRP laminate. The main findings from the present impacts test, which involved a low-velocity drop-weight impact test at an impact energy of 7.5 J on the centre of the specimen, are:

- The E-P, 3-D FEA model was able to predict accurately the load versus time, load versus displacement and energy versus time responses of the pristine and the patch-repaired CFRP composite specimens under an impact load. The load drop, or change in gradient of load-displacement trace,

associated with the initiation of intralaminar damage and interlaminar cracking, was clearly evident in both the experimental results and in the modelling predictions.

- In this meso-scale E-P, 3-D FEA model it was basically assumed that cracks initiated in the CFRP at a nano-scale, in the matrix around fibres, and then triggered sub-micrometre intralaminar matrix cracks that initiated and propagated around the impact point. These processes were initially controlled by the plasticity of the matrix and were localised under an indentation that resulted in the CFRP from the strike by the impactor. These localised regions of intralaminar cracking then led to interlaminar cracking, i.e. delamination, between the neighbouring plies. These types of damage were successfully simulated in the model. The delaminations initiated between plies of different fibre orientations and propagated along the orientation of the ply beneath the delamination. The development of such interlaminar cracking damage is primarily responsible for the failure of CFRP laminates.
- The numerical model predicted accurately the formation of delaminations in both the pristine CFRP specimens and the CFRP patch of the patch-repaired specimens, and yielded details on the area, shape and location of the delaminations through the thicknesses of the CFRP laminates. Indeed, these predictions of interlaminar cracking in the CFRP have been shown to be in very good agreement with the experimental results, as measured using C-scan tests, and this observation therefore further validated the numerical model that has been developed.
- In the patch-repaired CFRP specimens, there was no indication from the experimental studies of any cracking in the adhesive and this observation was in agreement with the results from the FEA studies, which indeed predicted that no adhesive cracking would occur in the impacted patch-repaired specimens.
- Using a thickness for the CFRP patch of half the thickness of the parent CFRP panel produced delamination damage in the patch greater in extent than the pristine CFRP panel incurred. Nevertheless, the damage in the patch-repaired specimen was all contained within the CFRP patch and did not spread into the parent CFRP panel, to which the patch was adhesively-bonded. This demonstrated that the bonded CFRP repair patch fulfilled one of its primary purposes in preventing the initiation and growth of interlaminar cracking in the parent CFRP.

Acknowledgements

The authors would like to thank Polar Manufacturing Ltd. for their assistance in manufacturing the patch-repaired CFRP composite panels. The work reported in this paper was presented at The Royal Society 'Griffith Centenary Virtual Conference on September 20-21, 2021' organised by Dr. Kevin Kendall FRS,

Professor Anthony Kinloch FREng FRS, Professor Neil Alford MBE FREng and Dr. Siva Bohm. The recording of the presentation is available via The Royal Society website. We gratefully acknowledge the financial support from AVIC ASRI and COMAC, China.

References

1. Baker AA, Rose LRF, Jones R. 2002 Advances in the Bonded Composite Repair of Metallic Aircraft Structure. 1st ed. Amsterdam: Elsevier Science. (ISBN 978-0-08-042699-0)
2. Wang CH, Doung CN. 2016 Bonded Joints and Repairs to Composite Airframe Structures. London: Academic Press. (ISBN 978-0-12-417153-4)
3. Katnam KB, Da Silva LFM, Young .M. 2013 Bonded repair of composite aircraft structures: A review of scientific challenges and opportunities. *Prog. in Aero. Sci*. **61**, 26-42. (https://doi.org/10.1016/j.paerosci.2013.03.003)
4. Clyne TW, Hull D. 2019 An Introduction To Composite Materials. Third edition. Cambridge University Press. (ISBN 9780521860956).
5. Neogi A, Mitra N, Talreja R. 2018 Cavitation in epoxies under composite-like stress states. *Compos. A: Appl. Sci. Manuf.* **106**, 52-58. (https://doi.org/10.1016/j.compositesa.2017.12.003)
6. Qiu B, Li M, Zhang X, Chen Y, Zhou S, Liang M, Zou H. 2021 Carboxymethyl cellulose sizing repairs carbon fiber surface defects in epoxy composites. *Materials Chemistry and Physics* **258**, 123677. (https://doi.org/10.1016/j.matchemphys.2020.123677)
7. Kimura M, Watanabe T, Takeichi Y, Niwa Y. 2019 Nanoscopic origin of cracks in carbon fibre-reinforced plastic composites. *Sci. Rep.* **9**, 19300. (https://doi.org/10.1038/s41598-019-55904-2)
8. Topac OT, Gozluklu B, Gurses E, Coker D. 2017 Experimental and computational study of the damage process in CFRP composite beams under low-velocity impact. *Compos. A: Appl. Sci. Manuf.* **92**, 167-182. (https://doi.org/10.1016/j.compositesa.2016.06.023)
9. Shi Y, Pinna C, Soutis C. 2014 Modelling impact damage in composite laminates: A simulation of intra- and inter-laminar cracking. *Compos. Struct.* **114**, 10-19. (https://doi.org/10.1016/j.compstruct.2014.03.052)
10. Davies GAO, Zhang X. 1995 Impact Damage prediction in carbon composite structures. *International Journal of Impact Engineering* **16**, 149-170. (https://doi.org/10.1016/0734-743X(94)00039-Y)
11. Moura MD, Marques AT. 2002 Prediction of low velocity impact damage in carbon-epoxy laminates. *Compos. A: Appl. Sci. Manuf.* **33**, 361-368. (https://doi.org/10.1016/S1359-835X(01)00119-1)
12. Berton T, Najafi F, Veer Singh C. 2019 Development and implementation of a multi-scale model for matrix micro-cracking prediction in composite structures subjected to low velocity impact. *Compos. B: Eng.* **168**, 140-151. (https://doi.org/10.1016/j.compositesb.2018.12.033)
13. Johnson DJ. 1987 Structure-property relationships in carbon fibres. *Journal of Physics D: Applied Physics.* **20**, 286-291. (https://doi.org/10.1088/0022-3727/20/3/007)
14. Sun XC, Hallett SR. 2018 Failure mechanisms and damage evolution of laminated composites under compression after impact (CAI): Experimental and numerical study. *Compos. A: Appl. Sci. Manuf.* **104**, 41-59. (https://doi.org/10.1016/j.compositesa.2017.10.026)
15. Hall ZEC, Liu J, Brooks RA, Liu H, Crocker JWM, Joesbury AM, Harper LT, Blackman BRK, Kinloch AJ, Dear JP. 2021 An investigation into the effectiveness of patch repairs to restore the impact properties of carbon-fibre reinforced-plastic composites for aerostructure applications. *Eng. Fract. Mech*. Submitted.
16. Baker AA. 2011 Bonded repair of composite aircraft structures. *Wiley Enc. of Composites: Online Library*. (https://doi.org/10.1002/9781118097298.weoc018)
17. Liu H, Liu J, Ding Y, Zheng J, Kong X, Zhou J, Harper L, Blackman B.R.K, Kinloch A.J, Dear J.P. 2020 The behaviour of thermoplastic and thermoset carbon-fibre composites subjected to low-velocity and high-velocity impact. *Journal of Mater. Sci*. **55**, 15741-15768. (https://doi.org/10.1007/s10853-020-05133-0)

18. Liu H, Liu J, Ding Y, Hall ZEC, Kong X, Zhou J, Blackman BRK, Kinloch AJ, Dear JP. 2020 A three-dimensional elastic-plastic damage model for predicting the impact behaviour of fibre-reinforced polymer-matrix composites. *Compos. B: Eng.* **201**, 108389. (https://doi.org/10.1016/j.compositesb.2020.108389)

19. Cuesta Torrado JJ. 2018 Experimental analysis and numerical optimisation of the effect of trigger mechanism on the energy absorption capabilities of composite tubular structures under impact loading. MSc Thesis, Cranfield University, UK.

20. Ramji A, Xu Y, Yasaee M, Grasso M, Webb P. 2020 Delamination migration in CFRP laminates under mode I loading. *Compos. Sci. Technol.* **190**, 108067. (https://doi:10.1016/j.compscitech.2020.108067)

21. Ramji A, Xu Y, Yasaee M, Grasso M, Webb P. 2021, Influence of veil interleave distribution on the delamination resistance of cross-ply CFRP laminates under low velocity impact. *Journal of Impact Engineering* **157**,103997. (https://doi.org/10.1016/j.ijimpeng.2021.103997)

22. Abir MR, Tay TE, Ridha M, Lee HP. 2017 On the relationship between failure mechanism and compression after impact (CAI) strength in composites. *Compos. Struct.* **217**, 242–250. (https://doi:10.1016/j.compstruct.2017.09.038)

23. Liljedahl CDM, Crocombe AD, Wahab MA, Ashcroft IA. 2007 Modelling the environmental degradation of adhesively bonded aluminium and composite joints using a CZM approach. *Intern. Journal of Adhesion Adhesives* **27**, 505-518. (https://doi.org/10.1016/j.ijadhadh.2006.09.015)

24. Blackman BRK, Dear JP, Kinloch AJ, MacGillivray H, Wang Y, Williams JG. 1995 The failure of fibre-composites and adhesively-bonded fibre-composites under high rates of test, Part I: Mode I loading - experimental studies*. Journal of Mater. Sci.* **30**, 5885–5900. (https://doi:10.1186/s40563-017-0087-7)

25. Dear JP, MacGillivray JH. Strain gauging for accurate determination of K and G in impact tests. 1992 *Journal of Mater. Sci*. **26**, 2124-32. (https://doi.org/10.1007/BF00549178)

26. Crouch BA, Williams JG. 1988 Modelling of dynamic crack propagation behaviour in the three-point bend impact specimen. *Journal of Mech. Phys. Solids* **36**, 1-13. (https://doi.org/10.1016/0022-5096(88)90017-8)

27. Williams JG, Adams GC. The analysis of instrumented impact tests using a mass-spring model. 1987 *Intern. Journal of Fract*. **33**, 209-222. (http://doi:org/10.1007/BF00013171)

28. Dear JP. 1990 High speed photography of impact effects in three-point bend testing of polymers. *Journal of Appl. Phys*. **67**, 4304-4312. (https://doi.org/10.1063/1.344946)

29. Bieniaś J, Jakubczak P, Surowska B. 2013 Comparison of polymer composites behavior to low-velocity impact and quasi-static indentation. *Compos. Theory Practice* **13**,155-159.